

# Production of hypernuclei with hadronic and electromagnetic probes

R. Shyam<sup>1,2</sup>

<sup>1</sup>Saha Institute of Nuclear Physics, Kolkata, India

<sup>2</sup>Institute für Theoretische Physik, Universität Giessen, Germany

February 9, 2022

## Abstract

We present an overview of a fully covariant formulation of describing the hypernuclear production with hadronic and electromagnetic probes. This theory is based on an effective Lagrangian picture and it focuses on production amplitudes that are described via creation, propagation and decay into relevant channel of  $N^*(1650)$ ,  $N^*(1710)$  and  $N^*(1720)$  intermediate baryonic resonance states in the initial collision of the projectile with one of the target nucleons. The bound state nucleon and hyperon wave functions are obtained by solving the Dirac equation with appropriate scalar and vector potentials. Specific examples are discussed for reactions which are of interest to current and future experiments on the hypernuclear production.

## 1 Introduction

Hypernuclei represent the first kind of flavored nuclei (with new quantum numbers) in the direction of other exotic nuclear systems (e.g., charmed nuclei). They introduce a new dimension to the traditional world of atomic nuclei. With a new degrees of freedom (the strangeness), they provide a better opportunity to investigate the structure of atomic nuclei [1]. For example, since the  $\Lambda$  hyperon does not suffer from the restrictions of the Pauli's exclusion principle, it can occupy all the states which are already filled up by the nucleons right upto the center of the nucleus. This makes it an unique tool to investigate the structure of the deeply bound nuclear states (see, e.g., [2, 3]). The data on the hypernuclear spectroscopy have been used extensively to extract information about the hyperon-nucleon ( $YN$ ) interaction within a variety of theoretical approaches [4, 5].

$\Lambda$  hypernuclei can be produced by beams of mesons, protons and also heavy ions. Very recently, it has become possible to produce them also with the electromagnetic probes like photons and electrons. Although, the stopped as well as in-flight ( $K^-$ ,  $\pi^-$ ) [6, 3] and ( $\pi^+$ ,  $K^+$ ) [6, 3, 2] reactions have been the most extensively used, the feasibility of producing hypernuclei via the ( $p$ ,  $K^+$ ), ( $\gamma$ ,  $K^+$ ) and ( $e$ ,  $e'K^+$ ) reactions has also been demonstrated in the recent years [7, 8, 9, 10, 11].

Several features of various hypernuclear production reactions can be understood by looking at the corresponding momentum transfers to the recoiling nucleus, since it controls to a great extent the population of the hypernuclear states. In Fig. 1, the momentum transferred to the recoiled nucleus is shown as a function of beam energy at two angles of the outgoing kaon for a number of reactions. We see that the ( $K^-$ ,  $\pi^-$ ) reaction allows only a small momentum transfer to the nucleus (at forward angles), thus there is a large probability of populating  $\Lambda$ -substitutional states in the residual hypernucleus ( $\Lambda$

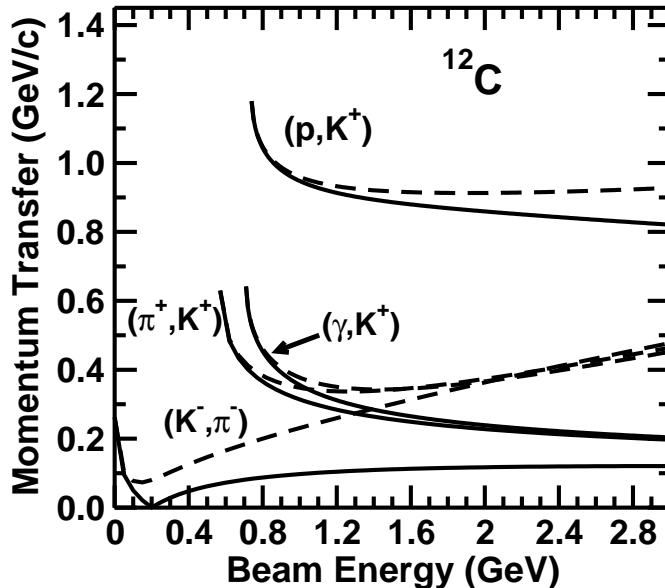


Figure 1: The momentum transfer involved in various hypernuclear production reactions as function of beam energy for the outgoing kaon angles of  $0^\circ$  (full lines) and  $10^\circ$  (dashed lines) for the  $^{12}\text{C}$  target.

occupies the same angular momentum state as that of the replaced neutron). On the other hand, in  $(\pi^+, K^+)$  and  $(\gamma, K^+)$  reactions the momentum transfers are larger than the nuclear Fermi momentum. Therefore, these reactions can populate states with configurations of a nucleon hole and a  $\Lambda$  hyperon in a series of orbits covering all bound states. The momentum transfers involved in the  $(p, K^+)$  reaction are still larger by a factor of about 3. Thus, the states of the hypernuclei excited in the  $(p, K^+)$  reaction may have a different type of configuration as compared to those excited in the  $(\pi^+, K^+)$  reaction. Nevertheless, it should be mentioned that usually larger momentum transfers are associated with smaller hypernuclear production cross sections. Each reaction has its own advantage and plays its own role in a complete understanding of the hypernuclear spectroscopy.

With the recent successful completion of experiments at Jlab which produced discrete hypernuclear states with electrons on  $^7\text{Li}$  and  $^{12}\text{C}$  targets for the first time [10, 11, 12] and with more such experiments planned at Jlab and also at the accelerators MAMI-C and ELSA [13], the exploration of the hypernuclei with electromagnetic probes has become of great current interest. In contrast to the hadronic reactions  $[(K^-, \pi^-)$  and  $(\pi^+, K^+)]$  which take place mostly at the nuclear surface due to strong absorption of both  $K^-$  and  $\pi^\pm$ , the  $(\gamma, K^+)$  and  $(e, e'K^+)$  reactions occur deep in the nuclear interior since  $K^+$ -nucleus interaction is weaker. Thus, this reaction is an ideal tool for studying the deeply bound hypernuclear states if the corresponding production mechanism is reasonably well understood. While hadronic reactions excite predominantly the natural parity hypernuclear states, both unnatural and natural parity states are excited with comparable strength in the electromagnetic reactions [14, 15, 16, 17]. This is due to the fact that sizable spin-flip amplitudes are present in the elementary photo-kaon production reaction,  $p(\gamma, K^+)\Lambda$ , since the photon has spin 1. This feature persists in the hypernuclear photo- and electro-production. Furthermore, since in these reactions a proton in the target nucleus is converted into a hyperon, it leads to the production of neutron rich hypernuclei (see, e.g., Ref. [18]) which may carry exotic features such as a halo structure. It can produce many mirror hypernuclear systems which would enable the study of the charge symmetry breaking with strangeness degrees of freedom.

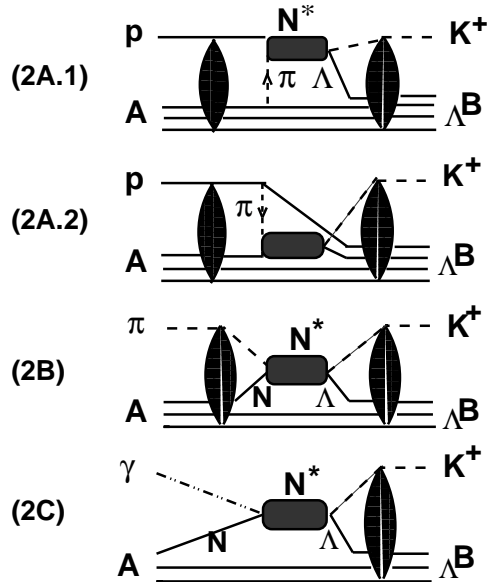


Figure 2: Types of the Feynman diagrams included in calculations of various reactions. In case of the  $(p, K^+)$  reaction two types of diagrams, the target emission (Fig. 2A.1) and projectile emission (Fig. 2A.2) contribute to the total amplitude. The elliptic shaded areas represent the optical model interactions in the incoming or outgoing channels

## 2 Covariant hypernuclear production amplitudes

Since we are still far way from calculations of the intermediate energy scattering and reactions directly from the lattice QCD, the effective field theoretical description in terms of the baryonic and mesonic degrees of freedom, is usually employed to describe these processes. These approaches introduce the baryonic resonance states explicitly in their framework and QCD is assumed to provide justification for the parameters or the cut-off functions used in calculations.

We use the diagrams shown in Fig. 2 for the calculations of the proton, meson and photon induced hypernuclear production reactions. In all the three cases, the initial state interaction of the projectile with a bound nucleon of the target leads to excitations of  $N^*(1650)[\frac{1}{2}^-]$ ,  $N^*(1710)[\frac{1}{2}^+]$ , and  $N^*(1720)[\frac{3}{2}^+]$  baryonic resonance intermediate states which decay into kaon and the  $\Lambda$  hyperon which gets captured into one of the nuclear orbits. These resonances have appreciable branching ratios for the decay into the  $K^+\Lambda$  channel and are known to contribute predominantly to the corresponding elementary reactions involved in various processes [19, 20].

To evaluate the amplitudes corresponding to the diagrams shown in Fig. 2, we require effective Lagrangians for the hadronic and electromagnetic couplings of the resonances. These are described in Refs. [8, 21]. The coupling constants at various interaction vertices, propagators for the intermediate resonance states and the form factors for the resonance-nucleon-meson vertices are all described in Refs. [8, 21, 22]. In the case of the  $(p, K^+)$  reaction the initial interaction between the incoming proton and a bound nucleon of the target is modeled by means of  $\pi$ ,  $\rho$  and  $\omega$  exchange mechanisms as discussed in Ref. [8]. Terms corresponding to the interference between various amplitudes are retained in the production amplitudes. Since calculations within this theory are carried out in the momentum space all along, they includes all the nonlocalities in the production amplitude that arises from the resonance propagators.

A crucial input required in the calculations of the  $(p, K^+)$  hypernuclear production reaction is the pion self-energy  $[\Pi(q)]$  which takes into account the medium effects on the intermediate pion propaga-

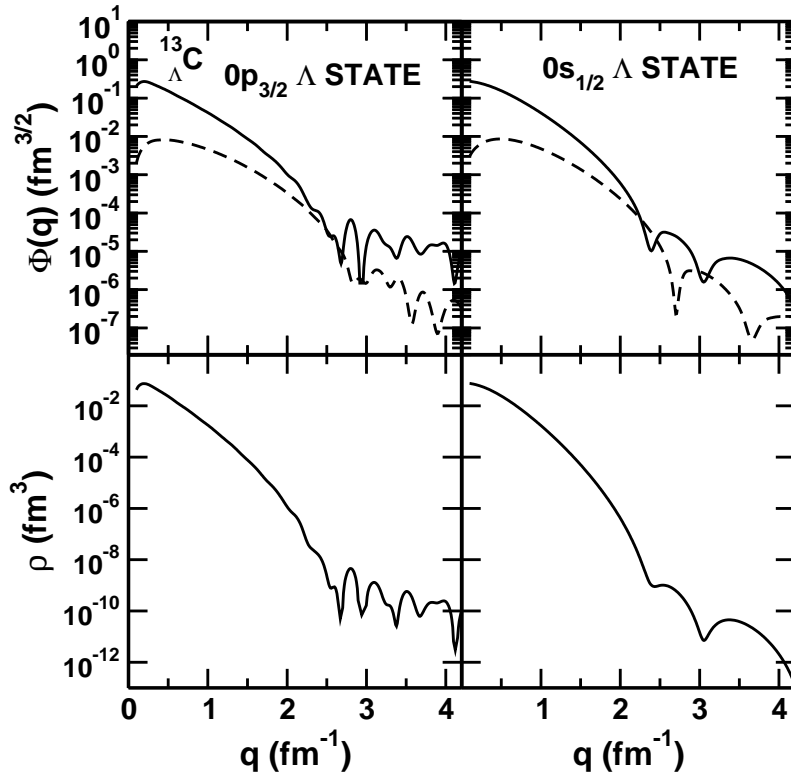


Figure 3: (Upper panel) Momentum space spinors  $[\Phi(q)]$  for the  $0p_{3/2}$  and  $0s_{1/2}$   $\Lambda$  orbits in  $^{13}_{\Lambda}\text{C}$  hypernucleus.  $|F(q)|$  and  $|G(q)|$  are the upper and lower components of the spinor, respectively. (Lower panel) Momentum distribution  $[\rho(q) = |F(q)|^2 + |G(q)|^2]$  for the same hyperon state calculated with these wave functions.

tion. Since the energy and momentum carried by such a pion can be quite large (particularly at higher proton incident energies), the calculation of  $\Pi(q)$  within a relativistic approach is mandatory. In our calculations of  $\Pi(q)$ , we take into account the contributions from the particle-hole ( $ph$ ) and delta-hole ( $\Delta h$ ) excitations produced by the propagating pions [23]. The self-energy has been renormalized by including the short-range repulsion effects through the constant Landau-Migdal parameter  $g'$  which is taken to be the same for  $ph - ph$  and  $\Delta h - ph$  and  $\Delta h - \Delta h$  correlations which is a common choice.  $g'$  acting in the spin-isospin channels, is supposed to mock up the complicated density dependent effective interaction between particles and holes in the nuclear medium. Most estimates give a value of  $g'$  between 0.5-0.7.

### 3 Results and Discussions

The spinors for the final bound hypernuclear state and for intermediate nucleonic states are required to perform numerical calculations of various amplitudes. We assume these states to have pure-single particle or single-hole configurations. The spinors in the momentum space are obtained by Fourier transformation of the corresponding coordinate space spinors which are the solutions of the Dirac equation with potential fields consisting of an attractive scalar part ( $V_s$ ) and a repulsive vector part ( $V_v$ ) having a Woods-Saxon form. The parameters of these potentials are given in Refs. [8, 21].

In Fig. 3, we show the lower and upper components of the Dirac spinors in momentum space for  $0p_{3/2}$  and  $0s_{1/2}$  hyperons in  $^{13}_{\Lambda}\text{C}$ . In each case, we note that only for momenta  $< 1.5 \text{ fm}^{-1}$ , is the lower

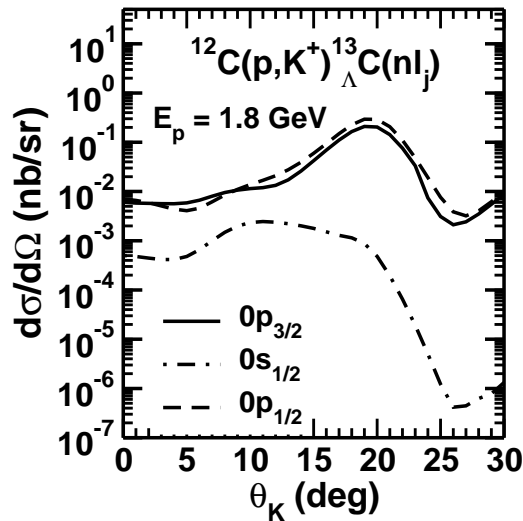


Figure 4: Differential cross section for the  $^{12}\text{C}(p, K^+)^{13}_{\Lambda}\text{C}$  reaction for the incident proton energy of 1.8 GeV for various bound states of final hypernucleus as indicated in the figure.

component of the spinor substantially smaller than the upper component. In the region of momentum transfer pertinent to exclusive kaon production, the lower components of the spinors are not negligible as compared to the upper component. This clearly demonstrates that a fully relativistic approach is essential for an accurate description of this reaction. The spinors calculated in this way provide a good description of the experimental nucleon momentum distributions for various nucleon orbits as is shown in Ref. [24]. In the lower panels of Fig. 3 we show momentum distribution,  $\rho(q) [= |F(q)|^2 + |G(q)|^2]$ , of the corresponding  $\Lambda$  hyperon. In each case the momentum density of the hyperon shell, in the momentum region around 0.35 GeV/c, is at least 2-3 orders of magnitude larger than that around 1.0 GeV/c. Thus reactions involving lower momentum transfers are expected to have larger cross sections.

In Fig. 4, we show the kaon angular distributions for various final hypernuclear states excited in the reaction  $^{12}\text{C}(p, K^+)^{13}_{\Lambda}\text{C}$ . We have used the plane waves to describe the scattering wave functions in the initial and final channels. The incident proton energy is taken to be 1.8 GeV where the angle integrated cross sections for this reaction has a maximum. We have used  $g' = 0.5$  in these calculations. The results are the coherent sum of all the amplitudes corresponding to the various meson exchange processes and intermediate resonant states. Clearly, the cross sections are quite selective about the excited hypernuclear state, being maximum for the state of largest orbital angular momentum. This is a direct reflection of the large momentum transfer involved in this reaction.

We note that the angular distributions have a maximum at angles larger than  $0^\circ$ . This can be understood by noticing that the bound state spinors of  $^{13}_{\Lambda}\text{C}$ , have several maxima in the upper and lower components in the region of large momentum transfers. Therefore, in the kaon angular distribution the first maximum may shift to larger angles reflecting the fact that the bound state wave functions show diffractive structure at higher momentum transfers. Furthermore, there is a difference of more than an order of magnitude between the cross sections for the  $p$ -shell and the  $s$ -shell excitations. This is a direct reflection of the fact that the binding energies ( $\varepsilon$ ) of the  $p$ -shell states are in the range of only 0.7-0.9 MeV as compared to 11.70 MeV of the  $s$ -shell. The bound state spinors behave at larger momentum transfers, approximately as  $\frac{1}{k^2}$  with  $k \propto \varepsilon$ . Thus, with increasing binding energies the magnitude of  $\Phi$  decreases, leading to the corresponding decrease in the cross sections. Therefore, the  $p$ -shell transitions are enhanced as compared to the  $s$ -shell one.

In Fig. 5, we show the dependence of our calculated cross sections on pion self-energy. It is interesting to note that this has a rather large effect. We also note a surprisingly large effect on the short range

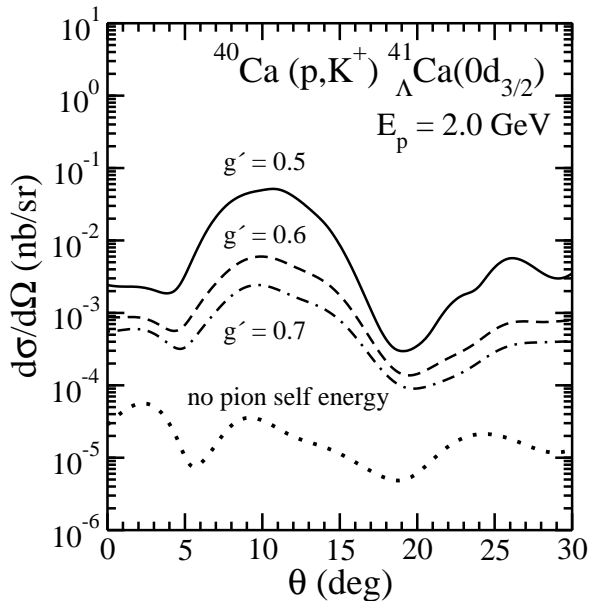


Figure 5: Differential cross section for the  $^{40}\text{Ca}(p, K^+)^{41}_{\Lambda}\text{Ca}(0d_{3/2})$  reaction for the incident proton energy of 2.0 GeV. The dotted line shows the results obtained without including the pion self-energy in the denominator of the pion propagator while full, dashed and dash-dotted lines represent the same calculated with pion self-energy renormalized with Landau-Migdal parameter of 0.5, 0.6 and 0.7, respectively.

correlation (expressed schematically by the Landau- Migdal parameter  $g'$ ). Similar results have also been reported in case of the  $(p, \pi)$  reactions [24].

In Fig. 6, we present the total cross sections for populating  $(0p_{3/2}^{-1}, 0p_{3/2}^{\Lambda})3^+, 2^+, 0^+$  states in the  $^{16}\text{O}(\gamma, K^+)^{16}_{\Lambda}\text{N}$  reaction as a function of photon energy. The contributions of all the resonances are coherently summed in the depicted cross sections. The distortion effects are ignored in the  $K^+$  channel; these effects are weak for  $(\gamma, K^+)$  reaction on lighter targets [14, 25]. A noteworthy aspect of this figure is that cross sections peak at photon energies around 900 MeV, which is about 200 MeV above the production threshold for this reaction. Interestingly, the total cross section of the elementary  $p(\gamma, K^+)\Lambda$  reaction also peaks about the same energy above the corresponding production threshold ( 910 MeV). Cross sections near the peak position are about 20 nb which should be measurable at MAMI-C and ELSA accelerator facilities.

We see in Fig. 6 that the highest  $J$  state is most strongly excited. From kinematical considerations it is easy to note that for large momentum transfer the orbital angular momentum transfer will also be large. Furthermore, we note that the cross section of the unnatural parity state  $3^+$  is larger than that of the natural parity state  $2^+$  by about a factor of 2.5 and by more than an order of magnitude than that of the  $0^+$  state. The unnatural parity states are excited through the spin flip process. Thus, kaon photoproduction on nuclei is an ideal tool for probing the structure of the unnatural parity hypernuclear states. The addition of unnatural parity states to the spectrum of hypernuclei is expected to constrain the spin dependent part of the effective  $\Lambda - N$  interaction more tightly. Within our formalism, the measured differential cross sections for the  $(\gamma, K^+)$  reaction can be used to probe directly the bound  $\Lambda$  wave functions provided the distortion effects in the kaon channels are weak and the nucleon bound state wave function is well controlled from the  $(e, e'p)$  data. Such information may prove to be very useful in certain cases where adding a  $\Lambda$  particle to the nucleus can lead to significant rearrangements in the structure of the nucleus. Such a possibility is discussed in Ref. [26].

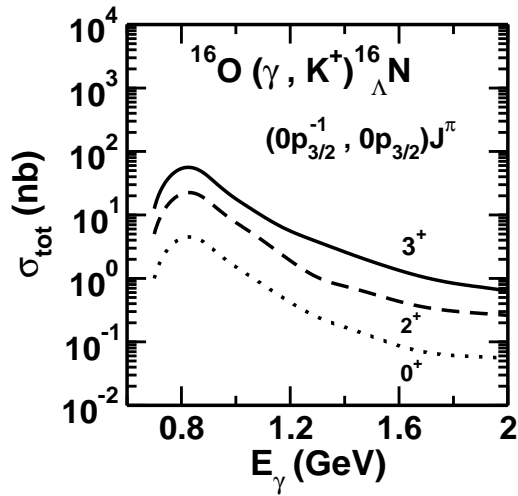


Figure 6: Total cross section for the  $^{16}\text{O}(\gamma, K^+)^{16}_{\Lambda}\text{N}$  reaction as a function of photon energy. Results are shown for various states corresponding to the  $(0p_{3/2}^{-1}, 0p_{3/2}^{\Lambda})J^{\pi}$  configuration.

We find that both  $(\gamma, K^+)$  and  $(p, K^+)$  reactions are dominated by the excitation of the positive parity spin- $\frac{1}{2}$   $N^*(1710)$  intermediate resonance state. The contributions of spin- $\frac{3}{2}$   $N^*(1720)$  state is almost negligible in both the cases (see also Refs. [23, 21]).

## 4 Summary and Conclusions

In summary, it is clear that the hypernuclear spectroscopy is indispensable for the quantitative understanding of the  $\Lambda$  hypernuclear structure and the  $\Lambda N$  interaction. Driven by the new proton and electron accelerator facilities, the field of hypernuclear production with protons, photons and electrons is expected to experience a grand revival. Already some data on the electron induced reactions are available from JLab and data on photon induced reactions are expected to be available in near future from MAMI-C and ELSA facilities. At the same times, our understanding of the hypernuclear production mechanism has improved significantly over the last decade.

A fully relativistic approach is essential for an accurate description of the hypernuclear production cross sections. It is feasible to calculate the reactions induced by hadronic and electromagnetic probes within a single fully covariant effective Lagrangian picture. Since the relevant elementary production cross sections are also described within the similar picture, most of the input parameters needed for the calculations of the hypernuclear production are fixed independently.

The calculated  $(p, K^+)$  cross sections are maximum for the hypernuclear state with the least binding energy and largest orbital angular momentum. The angular distributions for the favored transitions peak at angles larger than  $0^\circ$  which in contrast to the results of most of the previous nonrelativistic calculations for this reaction. This reflects directly the nature of the Dirac spinors for the bound states which involve several maxima in the region of large momentum transfers. The nuclear medium corrections to the intermediate pion propagator introduce large effects on the kaon differential cross sections. There is also the sensitivity of the cross sections to the short-range correlation parameter  $g'$  in the pion self-energy. Thus,  $(p, K^+)$  reactions may provide an interesting tool to investigate medium corrections on the pion propagation in nuclei.

The  $(\gamma, K^+)$  reaction selectively excites the high spin unnatural parity states. Thus kaon photoproduction on nuclei is an ideal tool for investigating the spin-flip transitions which are only weakly excited

in reactions induced by hadronic probes. Therefore, electromagnetic hypernuclear production provides a fuller knowledge of hypernuclear spectra which are used to investigate the details of the effective hyperon-nucleon interaction in the nuclear matter. A complete information about this spectrum will impose more severe constraints on the models of the  $YN$  interaction, particularly on its poorly known spin dependent part. Therefore, measurements for this reaction at future electron accelerator facilities would have very exciting prospects.

The author wishes to thank Horst Lenske and Ulrich Mosel for their collaboration on this subject. This work has been supported by the Sonderforschungsbereich/Transregio 16, Bonn-Giessen-Bochum of the German Research Foundation. One of the authors (RS) acknowledges the support of Abdus Salam International Centre for Theoretical Physics in form of a senior associateship award.

## References

- [1] B. F. Gibson and E. V. Hungerford III, Phys. Rep. **257** 349 (1995).
- [2] O. Hashimoto, H. Tamura, Prog.Part.Nucl.Phys. **57** 564 (2006).
- [3] H. Bandō, T. Motoba and J. Žofka, Int. J. Mod. Phys. **5** 2021 (1990).
- [4] E. Hiyama, M. Kamimura, T. Motoba, T. Yamada, and Y. Yamamoto, Phys. Rev. Lett. **85** 270 (2000).
- [5] C. M. Keil and H. Lenske, Phys. Rev. C **66** 054307 (2002).
- [6] R. E. Chrien and C. B. Dover, Annu. Rev. Nucl. Part. Sci. **39** 113 (1989).
- [7] J. Kingler et al., Nucl. Phys. **A634** 325 (1998).
- [8] R. Shyam, H. Lenske, and U. Mosel, Nuc. Phys. **764** 313 (2006).
- [9] H. Yamazaki et al., Phys. Rev. C **52** R1157 (1995).
- [10] M. Iodice et al., Phys. Rev. Lett. **99** 052501 (2007).
- [11] L. Yuan et. al., Phys. Rev. C **73** 044607 (2006).
- [12] T. Miyoshi et al., Phys. Rev. Lett. **90** 232502 (2003).
- [13] J. Pochodzalla, Nucl. Phys. **A754** 430c (2005).
- [14] C. Bennhold and L.E. Wright, Phys. Rev. C **39** 927 (1989); *ibid* Phys. Lett. **B191** 11 (1987).
- [15] T. Motoba, M. Sotona, and K. Itonaga, Progr. Theo. Phys. (suppl) **117** 123 (1994).
- [16] T.-S. H. Lee, Z.-Y. Ma, B. Saghai, and H. Toki, Phys. Rev. C **58** 1551 (1998).
- [17] F.X. Lee, T. Mart, C. Benhold, H. Haberzettl, and L. E. Wright, Nucl. Phys. **A695** 237 (2001).
- [18] T. Bressani et al.,Nucl. Phys. **A754** 410c (2005).
- [19] R. Shyam, Phys. Rev. C **60** 055213 (1999).
- [20] V. Shklyar, H. Lenske and U. Mosel, Phys. Rev. C **72** 015210 (2005).
- [21] R. Shyam, H. Lenske, and U. Mosel, arXiv:0710.4888
- [22] R. Shyam, Phys. Rev. C **73** 035211 (2006).
- [23] R. Shyam, H. Lenske, and U. Mosel, Phys. Rev. C **69** 065205 (2004).
- [24] R. Shyam, W. Cassing and U. Mosel, Nucl. Phys. **A586** 557 (1995).
- [25] A. S. Rosenthal et al., Ann. Phys. (N.Y.) **184** 33 (1988).
- [26] E.Hiyama eta al., Phys. Rev. C **53** 2075 (1996).